Title

On the Connection between Continental-Scale Land Surface Processes and the Tropical Climate in a Coupled Ocean–Atmosphere–Land System

Journal

Journal of Climate, 26(22)

ISSN

0894-8755

Authors

Ma, Hsi-Yen
Mechoso, C Roberto
Xue, Yongkang
et al.

Publication Date

2013-11-15

DOI

10.1175/jcli-d-12-00819.1

Peer reviewed

On the Connection between Continental-Scale Land Surface Processes and the Tropical Climate in a Coupled Ocean–Atmosphere–Land System

HSI-YEN MA,* C. ROBERTO MECHOSO,+ YONGKANG XUE,# HENG XIAO,@ J. DAVID NEELIN,+ AND XUAN JI+

* *Program for Climate Model Diagnosis and Intercomparison, Lawrence Livermore National Laboratory, Livermore, California*
+ *Department of Atmospheric and Oceanic Sciences, University of California, Los Angeles, Los Angeles, California*
# *Department of Atmospheric and Oceanic Sciences, and Department of Geography, University of California, Los Angeles, Los Angeles, California*
@ *Atmospheric Sciences and Global Change Division, Pacific North National Laboratory, Richland, Washington*

(Manuscript received 20 November 2012, in final form 23 April 2013)

ABSTRACT

An evaluation is presented of the impact on tropical climate of continental-scale perturbations given by different representations of land surface processes (LSPs) in a general circulation model that includes atmosphere–ocean interactions. One representation is a simple land scheme, which specifies climatological albedos and soil moisture availability. The other representation is the more comprehensive Simplified Simple Biosphere Model, which allows for interactive soil moisture and vegetation biophysical processes.

The results demonstrate that such perturbations have strong impacts on the seasonal mean states and seasonal cycles of global precipitation, clouds, and surface air temperature. The impact is especially significant over the tropical Pacific Ocean. To explore the mechanisms for such impact, model experiments are performed with different LSP representations confined to selected continental-scale regions where strong interactions of climate–vegetation biophysical processes are present. The largest impact found over the tropical Pacific is mainly from perturbations in the tropical African continent where convective heating anomalies associated with perturbed surface heat fluxes trigger global teleconnections through equatorial wave dynamics. In the equatorial Pacific, the remote impacts of the convection anomalies are further enhanced by strong air–sea coupling between surface wind stress and upwelling, as well as by the effects of ocean memory. LSP perturbations over South America and Asia–Australia have much weaker global impacts. The results further suggest that correct representations of LSP, land use change, and associated changes in the deep convection over tropical Africa are crucial to reducing the uncertainty of future climate projections with global climate models under various climate change scenarios.

1. Introduction

The different representation of land surface processes (LSP) in general circulation models (GCMs), and/or the associated sensitivity to changes in land surface conditions, is among the principal contributors to the large spread and uncertainty of precipitation simulations or future projections over land (e.g., Henderson-Sellers et al. 2003; Boone et al. 2004; Koster et al. 2004; 2006; Seneviratne et al. 2006; Wei and Dirmeyer 2010; Wei et al. 2010; Xue et al. 2004, 2006, 2010; Martin and Levine 2012). The LSP has a first-order effect on local surface fluxes. Using a coupled ocean–atmosphere GCM (CGCM), Ma et al. (2013, hereafter MA13) further demonstrated that interactive soil moisture and vegetation biophysical processes (VBP) can have significant impacts on the mean climate and interannual variability over *both* land and ocean, especially in the tropical Pacific. In turn, changes in the mean climate of the oceans can affect the mean climate over the continents through feedback mechanisms. MA13 referred to the impact of those feedbacks as the LSP ''indirect effect.'' These effects can enhance the uncertainty of future climate prediction owing to changes in the distribution of vegetation and land use.

Several studies have identified the correspondence between regional LSP perturbations and associated changes

Corresponding author address: Hsi-Yen Ma, Program for Climate Model Diagnosis and Intercomparison, Lawrence Livermore National Laboratory, Mail Code L-103, 7000 East Avenue, Livermore, CA 94551-0808.
E-mail: ma21@llnl.gov

DOI: 10.1175/JCLI-D-12-00819.1

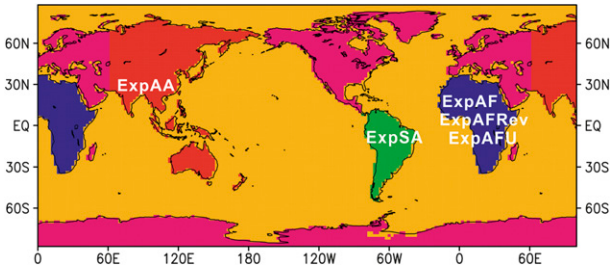

FIG. 1. Geographic map for the idealized regional land surface processes experiments. The land surface scheme, SSiB, in each CGCM experiment (ExpSA, ExpAA, or ExpAF) is replaced with the simple land scheme (SLS) only over the shaded region/model land grids (green, red, or blue). The AGCM-only ExpAFU has the same land scheme setup as ExpAF, and the ExpAFRev is CGCM with global SLS except SLS is replaced with SSiB over the African continent (blue shaded).

TABLE 1. List of CGCM land surface scheme experiments. Also see Fig. 1 for the geographic locations of each experiment.

Expt	Length (yr)	Description
CGCM/SLS	120	CGCM with global SLS
CGCM/SSiB	120	CGCM with global SSiB
AGCM/SSiB	20	AGCM with global SSiB
ExpSA	40	CGCM/SSiB except SLS over South American continent
ExpAA	40	CGCM/SSiB except SLS over Asian (East of 60°E) and Australian continent
ExpAF	70	CGCM/SSiB except SLS over African continent
ExpAFRev	40	CGCM/SLS except SSiB over African continent
ExpAFU	5	AGCM/SSiB except SLS over African continent

in atmospheric and oceanic conditions over the tropical oceans (e.g., Barnett et al. 1989; Meehl 1994; Zeng and Neelin 1999; Hu et al. 2004; Notaro et al. 2007; Richter et al. 2012; Swann et al. 2011). For example, both Barnett et al. (1989) and Meehl (1994) suggested, based on atmospheric GCM (AGCM) simulations, that a weaker South Asia monsoon associated with wetter and colder land surface conditions over the Asian continent could result in weaker surface wind stress and changes in surface heat fluxes over the tropical Pacific. Perturbations in regional land conditions over Asia therefore have the potential to affect the Pacific climate through their influence on monsoon convection. Fu and Wang (2003) further demonstrate the important roles of adjacent continental monsoon convection and air–sea coupling on the simulations of equatorial Pacific sea surface temperatures (SST) using a coupled atmosphere–ocean (Pacific-only) model of intermediate complexity. They argued that a better simulation of convection in association with Asian–Australian monsoons can improve the mean SST through enhancement in the strength of the trades and, thus, contribute to a correct semiannual cycle of surface wind speed and SST in the equatorial western Pacific. Zeng et al. (1996) and Richter et al. (2012) showed that either idealized or deforestation-mimicking perturbations in surface albedos can modify convection intensity over the continents (South America and Africa) adjacent to the Atlantic basin. The convection anomalies, in turn, can affect the low-level easterly trades of the Atlantic Walker circulation and underlying SSTs. Hales et al. (2004) noted strong precipitation sensitivity to leaf area index changes, especially in tropical Africa, occurring via both conductance and albedo effects.

The above studies reaffirm the important effects of convection anomalies on the large-scale circulation over land and ocean, especially for convection over major monsoon regions. Indeed, using two AGCMs and observed precipitation, Xue et al. (2010) quantitatively assessed the impact of interactive soil moisture and VBP on different regions over continents and found the impact to be most significant over the monsoon regions, especially in tropical Africa. These regions also correspond to those previously identified as strong coupling between precipitation and soil moisture, or the ''hot spots,'' in the Global Land–Atmosphere Coupling Experiment (GLACE) (Koster et al. 2004, 2006; Guo et al. 2006). MA13, based on a fully coupled CGCM, concluded that the improvements in the simulation of convection over the continents contribute to a more successful simulation of tropical climate in the Pacific basin. Significant changes in convection over land in MA13 approximately occur in regions of strong climate–VBP interactions over the global continents identified by Xue et al. (2010).

On the basis of the information on regions of strong climate–VBP interactions over the global continents, we have extended the work in MA13 to address an important unresolved issue: are the significant differences found between the simulations with different LSP parameterizations due primarily to the perturbations in a particular continental region with strong climate–VBP interactions or do they result from a superposition of effects from different such regions? The answer to this question can help to clarify the way in which regional LSPs impact the global climate. In the present paper, we follow the same methodology used by Ma et al. (2010), which compares GCM simulations with LSP perturbations given by different LSP parameterizations in selected continental regions. Our focus is on Africa, eastern Eurasia (east of 60°E) and Australia, and South America (Fig. 1).

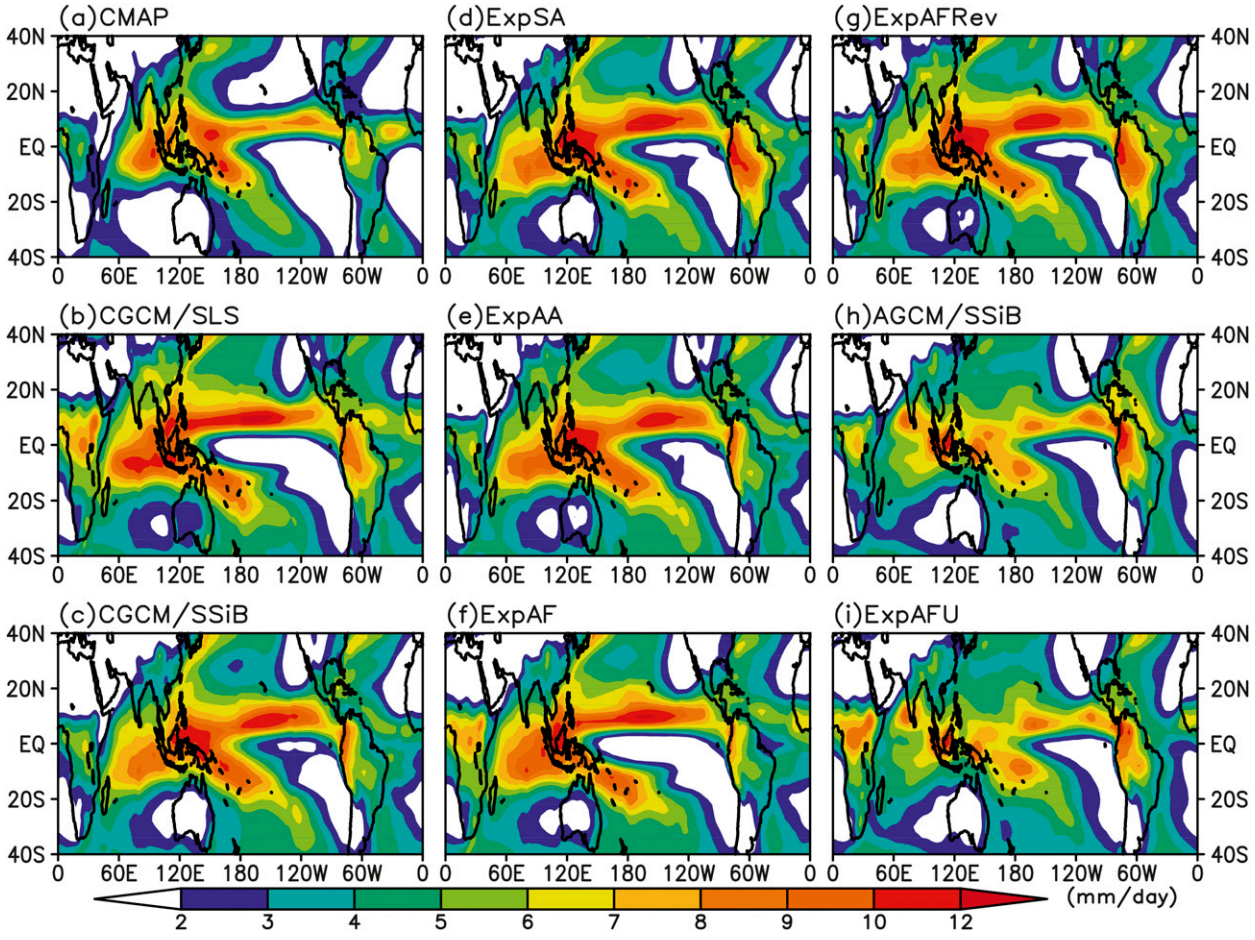

FIG. 2. Annual-mean precipitation (mm day^{-1}) from CMAP and all GCM simulations.

The remainder of the text is organized into four sections. Section 2 provides a brief introduction to the observational datasets and the CGCM, as well as the experimental setup. Section 3 examines the mechanisms for regional impact through a series of idealized LSP experiments. Section 4 presents a summary and our conclusions.

2. Datasets, model, and methodology

a. Observational datasets

We use monthly mean global precipitation fields from the Climate Prediction Center (CPC) Merged Analysis of Precipitation (CMAP) (Xie and Arkin 1997). CMAP, which merges observations from rain gauges and estimates from several satellite-based algorithms (infrared and microwave), covers the period 1979–2009. We also use monthly mean global SST fields from the National Oceanic and Atmospheric Administration (NOAA) extended reconstructed SST (ERSST), version 3b (v3b) (Smith et al. 2008). This dataset was compiled based on the International Comprehensive Ocean–Atmosphere dataset (ICOADS) SST data and on the application of improved statistical methods that allow for stable reconstruction using sparse data. The period used in this study covers from 1901 to 2000. (Both the CMAP and NOAA SST datasets are available online at http://www.esrl.noaa.gov/psd/.) We interpolated the fields in both datasets into a 2.0° latitude by 2.5° longitude grid to match the horizontal resolution of the AGCM.

b. Coupled atmosphere–ocean–land model

The CGCM used in this study is identical to that in MA13. The atmospheric component is the University of California, Los Angeles (UCLA) AGCM (Arakawa 2000; Mechoso et al. 2000). In the present study, we use the AGCM, version 7.1, with a horizontal resolution of 2.5° latitude and 2° longitude and 29 layers in the vertical. The distributions of greenhouse gases, sea ice, and ocean surface albedo are all prescribed corresponding to a monthly observed climatology.

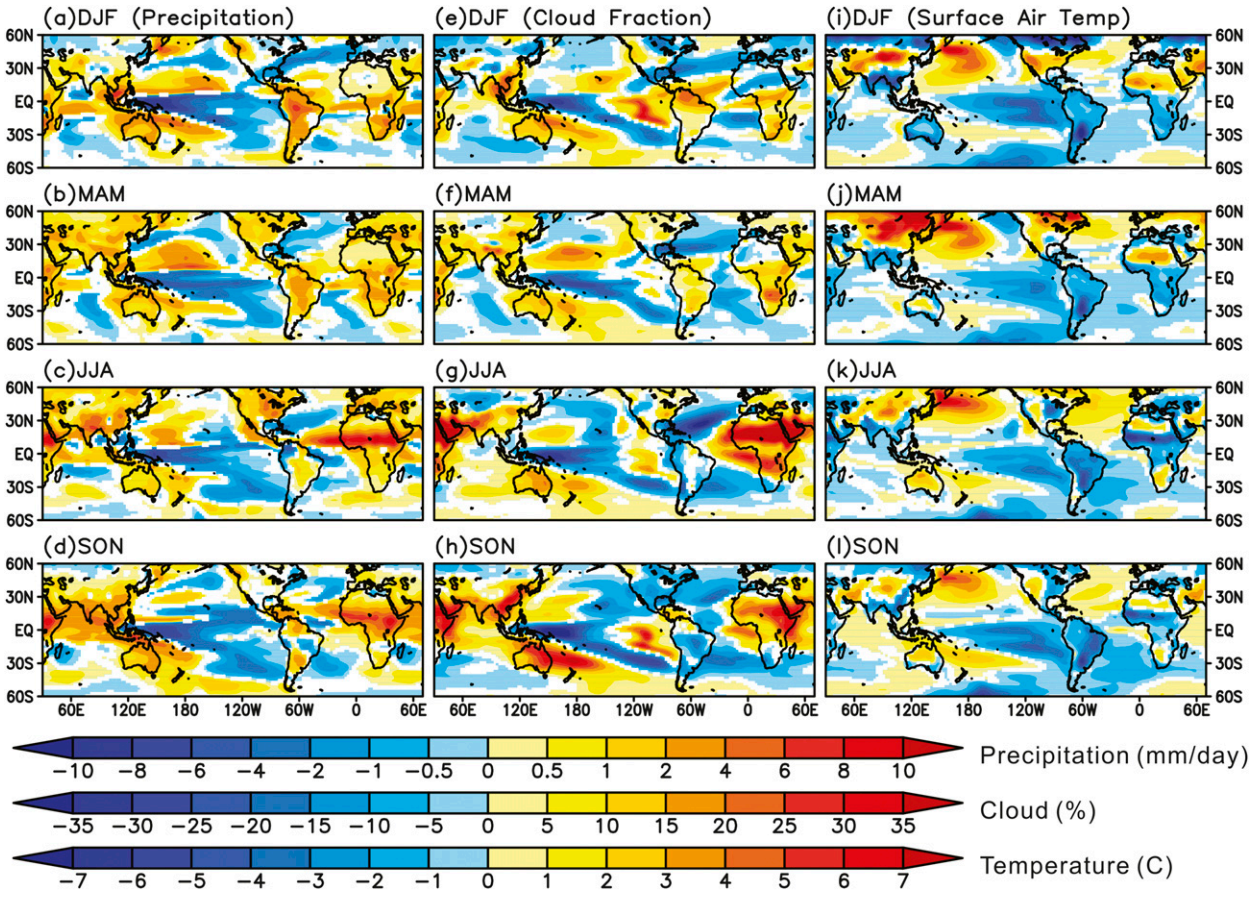

FIG. 3. (a)–(d) Differences of seasonal-mean precipitation (mm day^{-1}), (e)–(h) cloud fraction (%), and (i)–(l) surface air temperature (K) between CGCM/SLS and CGCM/SSiB (SLS minus SSiB). Regions where differences are statistically significant at the 95% confidence level are shaded.

The oceanic component is the Massachusetts Institute of Technology (MIT) GCM (Marshall et al. 1997; http://mitgcm.org). In the model configuration, the grid has 360 × 224 horizontal grid cells. Zonal grid spacing is 1° longitude, and meridional grid spacing is 0.3° latitude within ±10° of the equator increasing to 1° latitude poleward of 30°. There are 46 levels in the vertical with thicknesses ranging from 10 m near the surface to 400 m near the maximum depth of 5815 m. Ocean regions north of 73°N and south of 73°S are not represented in order to permit a 1-h integration time step.

Two choices of land surface components were utilized in this study: 1) a simple land scheme (SLS) that specifies most surface conditions/processes and 2) the first generation of the Simplified Simple Biosphere Model (SSiB) (Xue et al. 1991), which includes interactive land–atmosphere interactions. A detailed description of these two land schemes is presented in the appendix and a more detailed description of the model physics for the UCLA AGCM and MIT OGCM can be found in MA13. The atmospheric initial conditions for AGCM and CGCM experiments were taken from a previous multiyear model run starting from 1 October 1982. The oceanic initial conditions for the MIT GCM were taken from a multiyear model run of the experiments conducted in Cazes-Boezio et al. (2008). The reasonable CGCM performance was also demonstrated in MA13.

c. *Simulations and experiments*

Two 120-yr-long CGCM simulations, one with SLS (no interactive soil moisture/VBP) and the other with SSiB (interactive soil moisture/VBP), form our baseline simulations, and are referred to as CGCM/SLS and CGCM/SSiB. These two simulations are identical to those in MA13. The differences between the last 100 years of these simulations will serve as "control". We also performed three idealized CGCM experiments using the SSiB globally except in selected continental

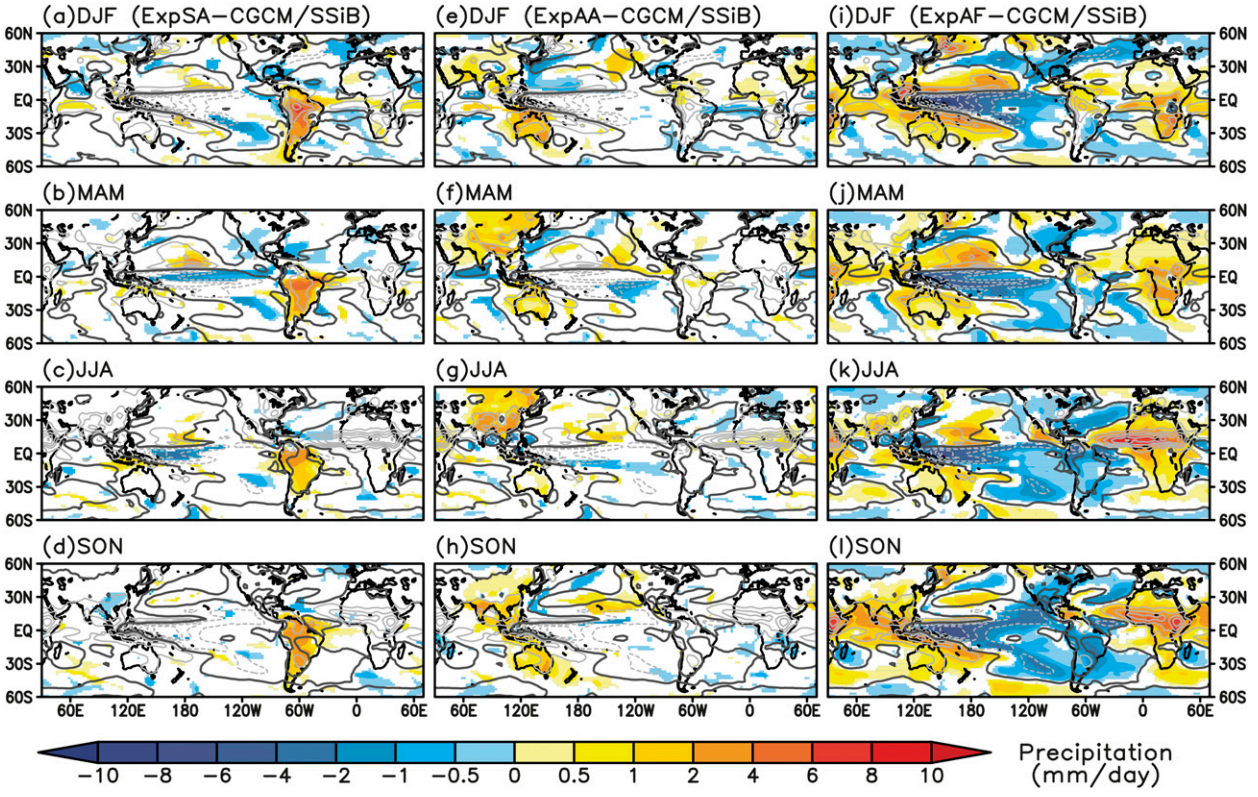

FIG. 4. Differences of seasonal-mean precipitation (mm day^{-1}) between (a)–(d) ExpSA, (d)–(h) ExpAA, (i)–(l) ExpAF and CGCM/SSiB (sensitivity experiments minus SSiB). Regions where differences are statistically significant at the 95% confidence level are shaded. Contours indicate the zero values of CGCM/SLS minus CGCM/SSiB (Fig. 3a–d) for each season.

regions where the SLS is used (see Table 1 and Fig. 1). The selected regions for the experiments are South America in ExpSA, eastern Eurasia (east of 60°E) and Australia in ExpAA, and Africa in ExpAF. A fourth experiment uses the SLS globally except in Africa where the SSiB is used (ExpAFRev). In all cases the results corresponding to the first 20 years will not be included in the analysis. The reason for focusing on the African continent is that the largest impacts mainly come from LSP perturbations in the African continent, as we will demonstrate later in section 3. We also performed another two experiments using the uncoupled AGCM: AGCM/SSiB and ExpAFU (SLS is used for Africa). The rationale for these AGCM experiments is given by our interest in assessing the importance of air–sea interactions in CGCM/SSiB and ExpAF. Figure 2 shows the annual mean precipitation from both CMAP and all GCM experiments. In general, the overall patterns of the simulated precipitation fields are reasonable compared to CMAP, although differences among the experiments can be found at regional scales due to the experiment setup.

3. Sensitivity of continental-scale land surface processes

a. *Sensitivity of seasonal-mean climatology and variability*

Figure 3 presents the seasonal-mean differences of precipitation, total cloud fraction, and surface air temperature between CGCM/SLS and CGCM/SSiB (SLS minus SSiB). Unlike in MA13, here we plot the differences obtained in the idealized experiments minus those in CGCM/SSiB. This is because the CGCM simulation with SSiB produces a better mean climatology and interannual variability than the simulation with SLS compared to observations. Figure 3 also serves as the ''control reference'' when we compare the results from the idealized experiments.

The differences in precipitation and total cloud fraction are generally larger in the tropics and subtropics than high latitudes both over land and ocean. The signs of the differences for a particular field are generally the same for all four seasons, although there is a strong seasonality in magnitude. Over land areas, precipitation is generally too high in CGCM/SLS mostly owing to

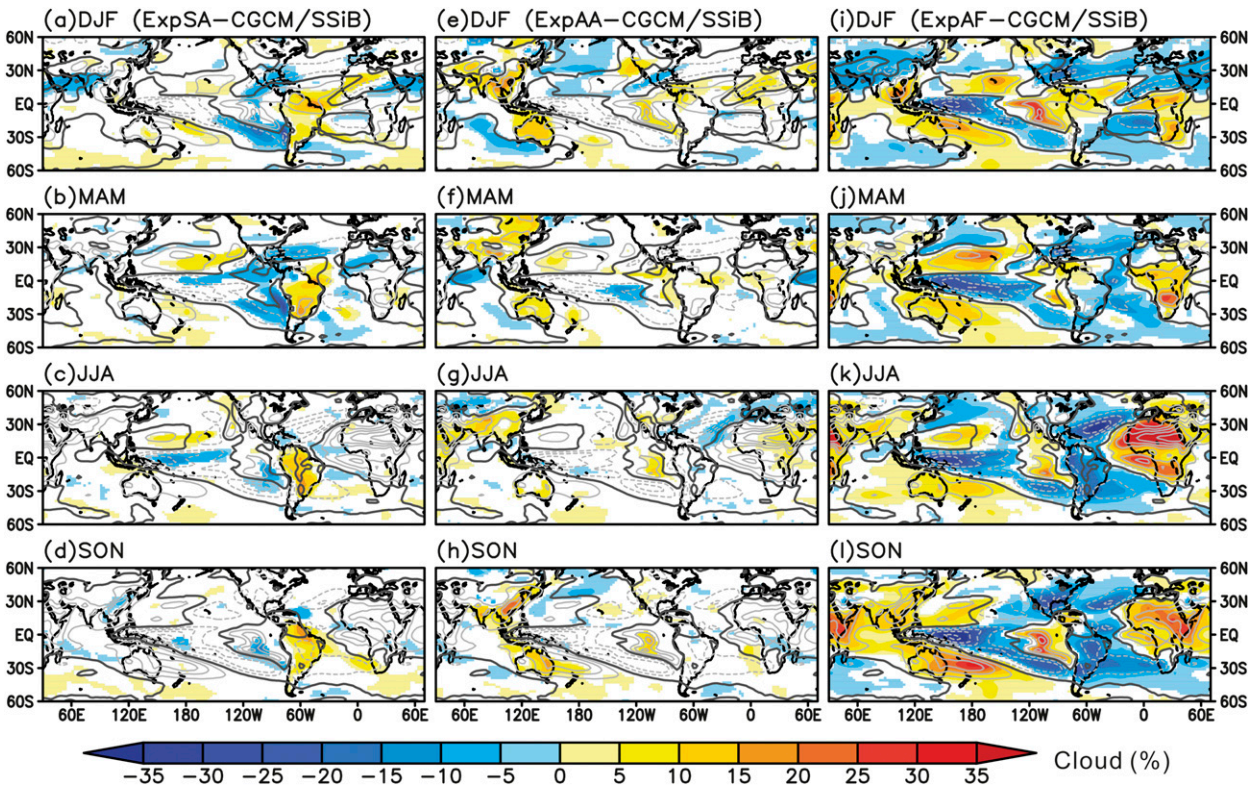

FIG. 5. As in Fig. 4, but for total cloud fraction (%).

higher latent and lower sensible heat fluxes [i.e., lower Bowen ratio, higher evaporation fraction, and more convective available potential energy (CAPE)]. There is also a strong seasonality over regions of strong climate–VBP interactions (Xue et al. 2010), such as tropical Africa, tropical South America, and South Asia. These regions are characterized by monsoon climates, and the differences over land are largest during the warm seasons [June–August (JJA) for the African and Indian monsoons and December–February (DJF) for the South American monsoon systems]. These regions also correspond to those previous identified as strong coupling between precipitation and soil moisture in the GLACE experiment. The interannual variability of precipitation over land is also changed, especially over regions of large precipitation mean differences (not shown here). Over the ocean, the spatial distribution of the differences varies significantly between CGCM/SLS and CGCM/SSiB, especially over the Pacific. In reference to CGCM/SSiB, CGCM/SLS has smaller precipitation mainly over the entire tropical Pacific basin with the largest differences over the western Pacific, while more precipitation in the subtropics in both hemispheres over the central and western Pacific. The changes in the Atlantic and Indian Ocean basins are smaller than those in the Pacific basin. Over the Atlantic, CGCM/SLS shows more precipitation over the northern tropics and subtropics as well as over the eastern tropical and subtropical Atlantic and less precipitation over the southern subtropical and midlatitudes. Over the Indian Ocean basin, CGCM/SLS generally shows more precipitation over the northern sector and smaller precipitation over the southern sector. The changes in precipitation are most likely due to changes in SSTs, which are modified by surface wind stress.

The differences in total cloud cover correspond to those in deep convection (precipitation) except for major marine stratocumulus regions (e.g., Peruvian and Namibian coasts). The larger differences in the cloud cover over the Peruvian stratocumulus region are in September–November (SON) and DJF, while over the Namibian stratocumulus region the differences are larger in JJA. The surface air temperature over land is generally colder in CGCM/SLS over deep convection regions and warmer over deserts in association with smaller sensible heat fluxes in the former regions and larger in the latter. Over the oceans, CGCM/SLS shows colder surface air temperatures over the tropical Pacific, especially over the southeastern Pacific, and warmer temperatures over the northern and southwestern Pacific,

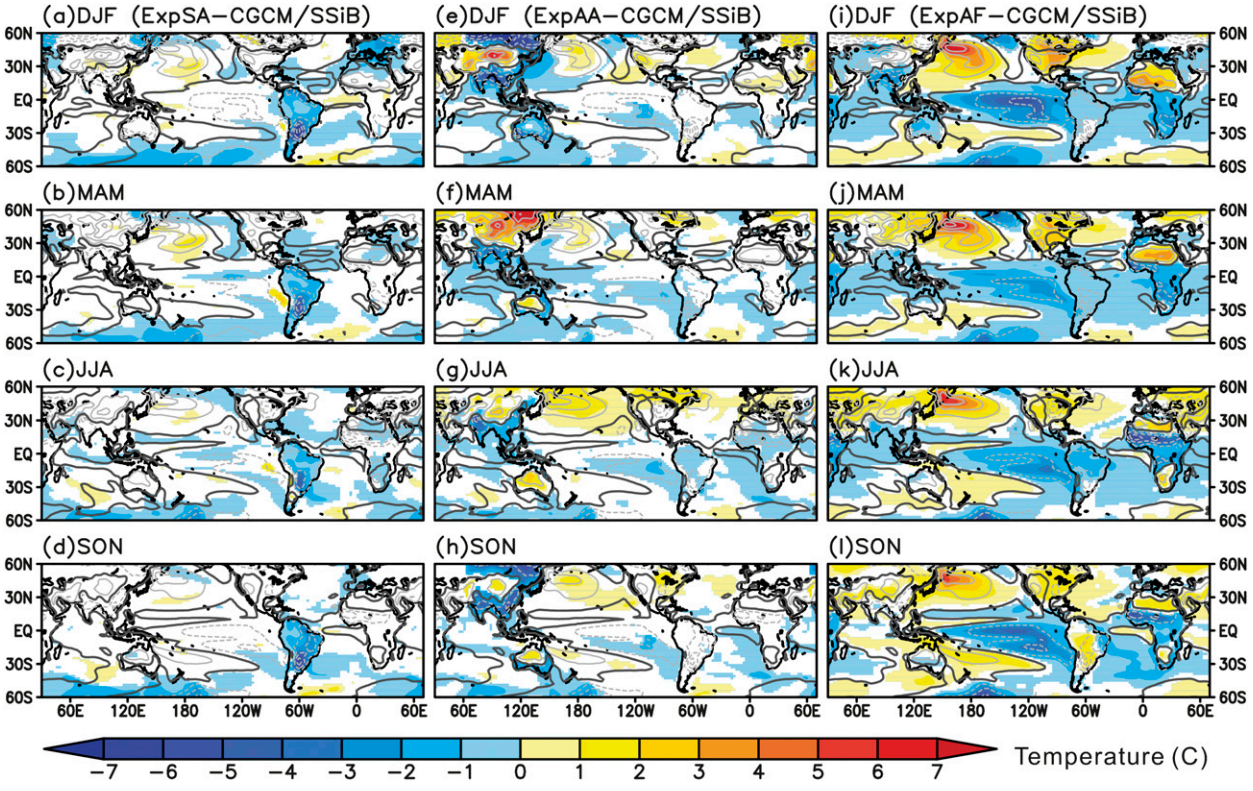

FIG. 6. As in Fig. 4, but for surface air temperature (°C).

eastern Indian Ocean, and North Atlantic. There is also strong seasonal variability over the eastern Pacific and the Asian continent in the midlatitudes.

The seasonal-mean precipitation differences between the idealized LSP experiments and CGCM/SSiB are shown in Fig. 4. We also plotted the zero contours of the differences between CGCM/SLS and CGCM/SSiB from Fig. 3 as the reference contours for each experiment. For ExpSA and ExpAA, the large precipitation differences with statistical significance at the 95% level are generally confined over the land regions where the land surface scheme was switched from SSiB to SLS. In ExpSA, the precipitation difference is largest in DJF and mostly confined over the South American continent. There are, however, some differences with statistical significance over the equatorial Pacific in MAM and JJA and over the equatorial Atlantic in DJF and MAM. In ExpAA, the precipitation differences are mainly over the eastern part of the Asian continent in March–May (MAM) and JJA, the Maritime Continent and Australia in SON and DJF, and with some differences over the North Pacific in DJF and MAM and the equatorial Pacific in JJA. The ExpAF, however, reproduced the majority of precipitation differences over the African continent and in the tropical Pacific, as seen in Fig. 3. The differences are larger in Africa during JJA and SON. The presence of precipitation differences in ExpAF over South America, East and South Asia, and Australia is interesting because this suggests that land surface processes over Africa can have a remote impact on other continents. The ExpAF shows more precipitation in all seasons over the Asian and Australian continents, except over Asia in DJF. The precipitation, however, is reduced over the South American continent in ExpAF, and differences are opposite to those in ExpSA.

Figures 5 and 6 show the differences of seasonal mean cloud fraction and surface air temperature between the three sensitivity experiments and CGCM/SSiB. Again, the largest differences and strong seasonal variations are present in the ExpAF over the African continent and Pacific basin for all the seasons, while both ExpSA and ExpAA generally show differences with statistical significance over the regions where land surface schemes are changed. In ExpAF, the LSPs over Africa also have a large impact on cloud fraction and surface air temperature over the continents of the Americas, Eurasia, and Australia. For cloud fraction, ExpAF shows more cloud amount over tropical South America in DJF and MAM, over Eurasia in MAM, JJA, and SON, and over Australia in all seasons. For all other land regions (the

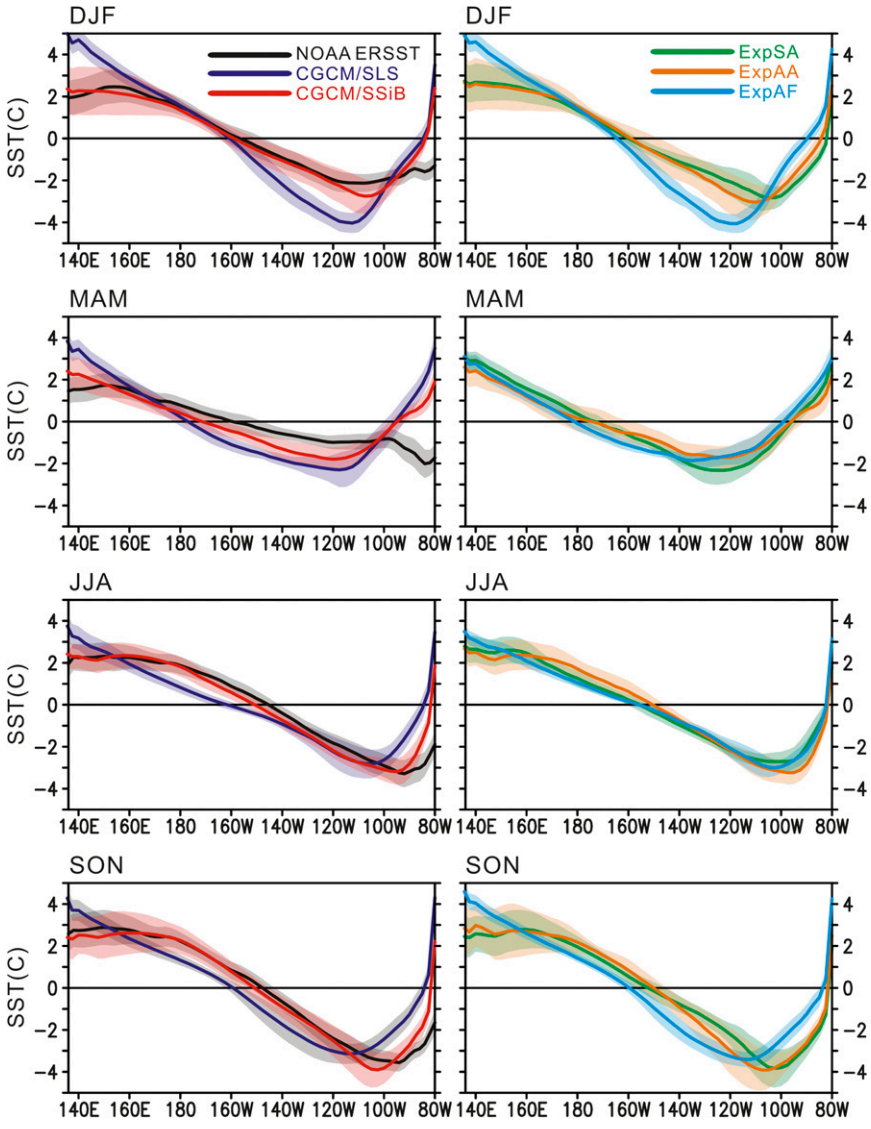

FIG. 7. Seasonal-mean SST deviation (°C) from the zonal mean averaged along the equator between 2°S and 2°N for the Pacific basin from (left) NOAA ERSST, CGCM/SLS, and CGCM/SSiB, as well as from (right) ExpSA, ExpAA, and ExpAF experiments. Shaded areas are the ±1 standard deviation of seasonal means.

Americas, Eurasia, and Australia) and seasons, ExpAF shows less cloud amount. For surface air temperature, ExpAF shows higher temperature over North America in all the seasons, over South America in SON, and over Eurasia (except South Asia) in MAM, JJA, and SON. For all other land regions and seasons, colder temperatures are present in ExpAF. We can also see in ExpSA that LSPs over Africa can have a significant impact on the Peruvian stratocumulus in DJF and MAM and also the cloud fraction over the eastern Atlantic. The changes in cloud fraction could result from changes in subsidence associated with South American monsoon systems (Rodwell and Hoskins 2001) and local air–sea interactions. For surface air temperature, ExpAA only shows large signals in the mid and high latitudes over the Asian continent in DJF and MAM, probably due to changes in the intensity of the Asian winter monsoon.

We next concentrate on the impact of regional LSPs on the tropical Pacific climate. Figure 7 presents the deviations from the zonal- and seasonal-mean SST along the equatorial Pacific from observations (NOAA ERSST), CGCM/SLS, CGCM/SSiB, ExpSA, ExpAA, and ExpAF. In observations, the SST deviation shows

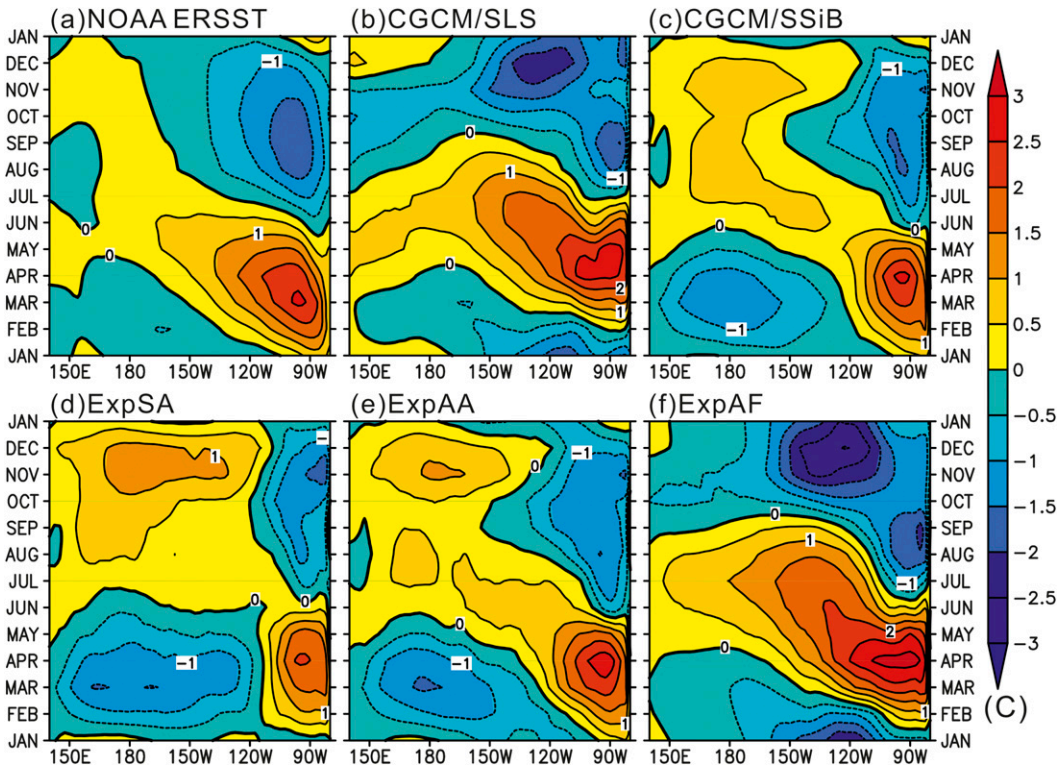

FIG. 8. Seasonal cycle of equatorial SST (°C) between 2°S and 2°N in terms of deviations from the annual mean for the Pacific basin from (a) NOAA ERSST, (b) CGCM/SLS, (c) CGCM/SSiB, (d) ExpSA, (e) ExpAA, and (f) ExpAF.

a strong zonal gradient between 160°E and 100°W in the Pacific basin with warm SST in the west and cold SST in the east in all seasons. The gradient is strongest in SON and weakest in MAM. In the simulations, CGCM/SSiB shows similar SST gradients to observations in DJF, JJA, and SON except over the eastern Pacific owing to the biases in stratocumulus clouds. The unrealistic SST gradient over the western Pacific warm pool in the CGCM/SLS is consistent with the stronger equatorial easterly trades (MA13). The SST gradient in either ExpSA or ExpAA is similar to that in CGCM/SSiB, suggesting that regional LSPs in these two regions have little impact on the SST gradient. The ExpAF, however, shows a large impact in both SON and DJF and has very a similar SST gradient to CGCM/SLS. The impact is smaller in JJA and MAM. In addition, the interannual variability (shaded area) of the SST gradient in ExpAF is also smaller compared to CGCM/SSiB, ExpSA, or ExpAA.

Figure 8 further displays the LSP impact on the seasonal cycle of SST along the equatorial Pacific (2°S–2°N). In the observations, the seasonal cycle of SST shows a strong east–west asymmetry with seasonal variations dominated by a semiannual harmonic in the west and by an annual harmonic variation in the east. The SST variations in the east show a warm phase in the first half of the year peaking in March, with a cold phase in the second half of the year peaking in September at about 100°W. These warm and cold phases of the equatorial cold tongue differ from each other in strength, duration, and propagation characteristics. Both phases exhibit a clear westward propagation in the observations, with the warm phase exhibiting higher amplitude (and shorter duration). In the model version, the CGCM/SSiB exhibits a better simulation of the seasonal cycle than does CGCM/SLS, compared to observations. For the LSP experiments, ExpSA resembles CGCM/SSiB in many aspects but has a later cold maximum in November, and the warm phase has weaker temperature anomalies over the eastern Pacific. It also shows little westward propagation of both warm and cold phases. For ExpAA, the LSP has little impact on the SST seasonal cycle in both the western and eastern Pacific for phases, magnitude, and westward propagation. For ExpAF, the result is very similar to CGCM/SLS, suggesting that the improvement seen in CGCM/SSiB is mainly from the impact of land surface processes over Africa. The results here again suggest the high sensitivity of tropical Pacific climate to the LSP over the African continent.

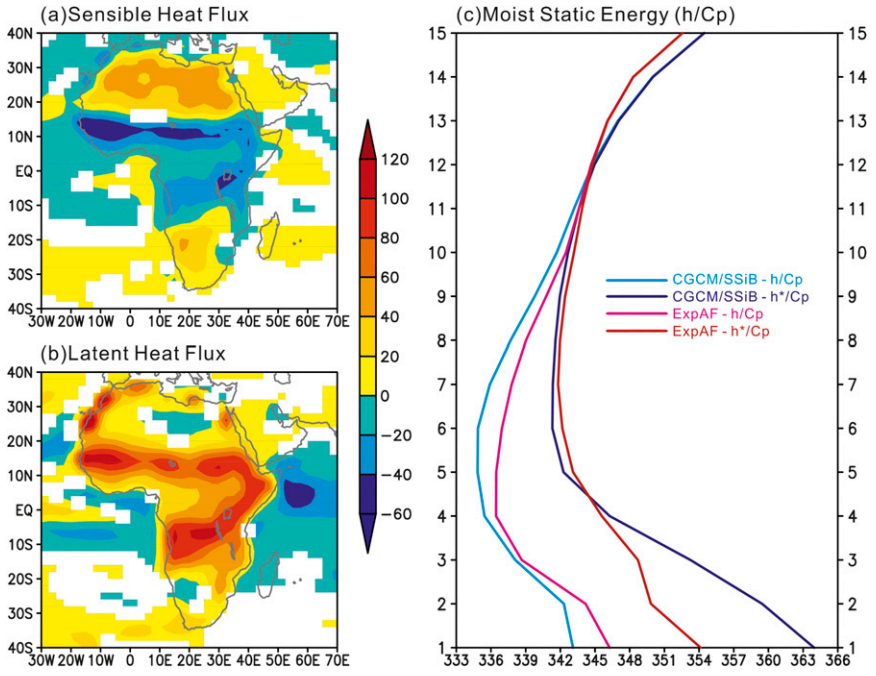

FIG. 9. Differences of June–August mean (a) sensible heat flux and (b) latent heat flux ($W\,m^{-2}$) between ExpAF and CGCM/SSiB (ExpAF minus SSiB). Regions where differences are statistically significant at the 95% confidence level are shaded. (c) Vertical profiles (in model sigma levels) of June–August mean moist static energy (h/c_p) and its saturated value (h^*/c_p) (K) normalized by specific heat (c_p) for CGCM/SSiB and ExpAF averaged between 0° and 15°N, 0° and 40°E. The first sigma level is the planetary boundary layer and the fifteenth level is the tropopause.

b. *Mechanisms for the connection between LSPs over Africa and the tropical Pacific climate*

The results presented in the previous section reveal a marked sensitivity of the mean and seasonal cycle of SSTs in the tropical Pacific to the LSP (interactive soil moisture and VBP) over the African continent. The LSP effects from other continents examined in this study only have secondary or minimal impact on the tropical Pacific climate. The key processes suggested by MA13 are as follows: 1) LSP perturbations modify the intensity of convection over land (Africa) and in turn change the large-scale circulation and 2) the equatorial easterly trades and surface zonal wind stress in the Pacific, as part of the large-scale flow, change interactively with the upper-ocean circulation, including the SST gradient and thermocline depth along the equator, as well as the equatorial seasonal cycle of SST and interannual variability. In this section, we propose possible mechanisms for the connection between LSP perturbations over the African continent and tropical Pacific climate.

We start by examining the changes in JJA surface fluxes and vertical profiles of moist static energy between ExpAF and CGCM/SSiB over the African continent (Fig. 9) since precipitation changes are largest in northern summer. In tropical Africa, ExpAF produces less sensible but more latent heat fluxes than CGCM/SSiB. These changes in surface fluxes result in a moister planetary boundary layer (PBL) and atmospheric column in ExpAF, as indicated by the moist static energy profiles (Fig. 9c). These profiles have considerably more CAPE in ExpAF; that is, the stronger convection and precipitation in ExpAF is consistent with a moister PBL and lower troposphere.

We further examine the changes in the large-scale circulation associated with the anomalies in convection over Africa. Figure 10 shows the differences of seasonal-mean divergent winds and velocity potential at 150 hPa between ExpAF and CGCM/SSiB (ExpAF minus CGCM/SSiB). The overall patterns are very similar to those between CGCM/SLS and CGCM/SSiB except that the overall magnitude of differences between CGCM/SLS and CGCM/SSiB is larger and another center of divergent flows associated with convection of the South American monsoon system is also present in DJF and MAM (not shown). In Fig. 10, there is a center of strong divergent flows associated with the anomalous

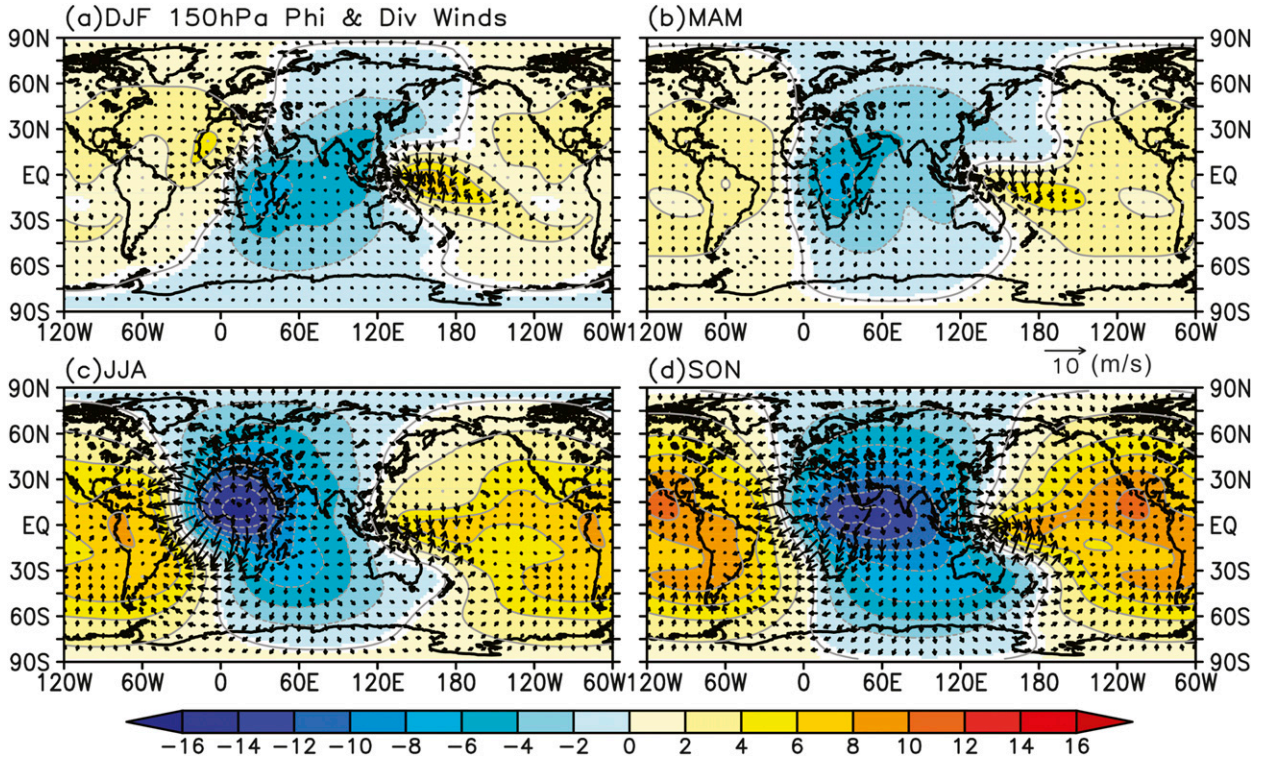

FIG. 10. Differences of seasonal-mean divergent winds ($m\,s^{-1}$, arrows) and velocity potential ($m^2\,s^{-1}$, color shading and contours) at 150 hPa between ExpAF and CGCM/SSiB. Regions and vectors where differences are statistically significant at the 95% confidence level are shaded and in dark black, respectively.

convection over tropical eastern Africa in all seasons. The largest differences in JJA and SON are associated with changes in African monsoon intensity, consistent with Figs. 4k and 4i. The convergent/sinking regions are likewise consistent with changes in precipitation, with strong sinking in the equatorial western Pacific as well as over the subtropical eastern Pacific and South Atlantic in JJA and SON. Figure 11 further shows the differences in seasonal-mean total velocity and streamfunction at 925 hPa between ExpAF and CGCM/SSiB. Again, the overall differences are very similar to those between CGCM/SLS and CGCM/SSiB (not shown here) except for smaller magnitudes in Fig. 11. For all of the seasons, significant changes are found in the subtropical highs in both the Pacific and Atlantic basins. The change is particularly clear in the South Pacific, where the subtropical high is stronger and has a more westward extension in ExpAF than in CGCM/SSiB. The equatorial easterly trades in the Pacific (Atlantic) are also stronger (weaker) in ExpAF for most seasons except in DJF. The largest changes in the subtropical highs in both Pacific and Atlantic Oceans are found during SON.

The differences shown in Figs. 10 and 11 over the tropics and subtropics largely resemble Gill's solution (Gill 1980) for the atmospheric response to anomalous convective heating slightly off the equator. One can anticipate therefore that the connection between the African convection and equatorial Pacific trades can be explained through equatorial wave dynamics. To further gain insights into the remote response to the convective heating in Africa, we apply a simple atmospheric model developed by Lee et al. (2009). This is a steady-state two-level primitive equation model, linearized about a prescribed background mean state. This model has been used in several theoretical studies by Lee et al. (2009) and Wang et al. (2010) on the impact of convection heating associated with the Atlantic warm pool. In this experiment, the prescribed mean states correspond to the large-scale flows at 250 and 750 hPa from the JJA climatology of the National Centers for Environmental Prediction–National Center for Atmospheric Research (NCEP–NCAR) reanalysis (Kalnay et al. 1996). A thermal forcing of Gaussian shape at middle level (500 hPa), where the intensity approximately corresponds to the heating difference between ExpAF and CGCM/SSiB ($\sim$2.5 K day^{-1}), is prescribed centered at 10°N, 25°E to mimic the anomalous convective heating. More details of model

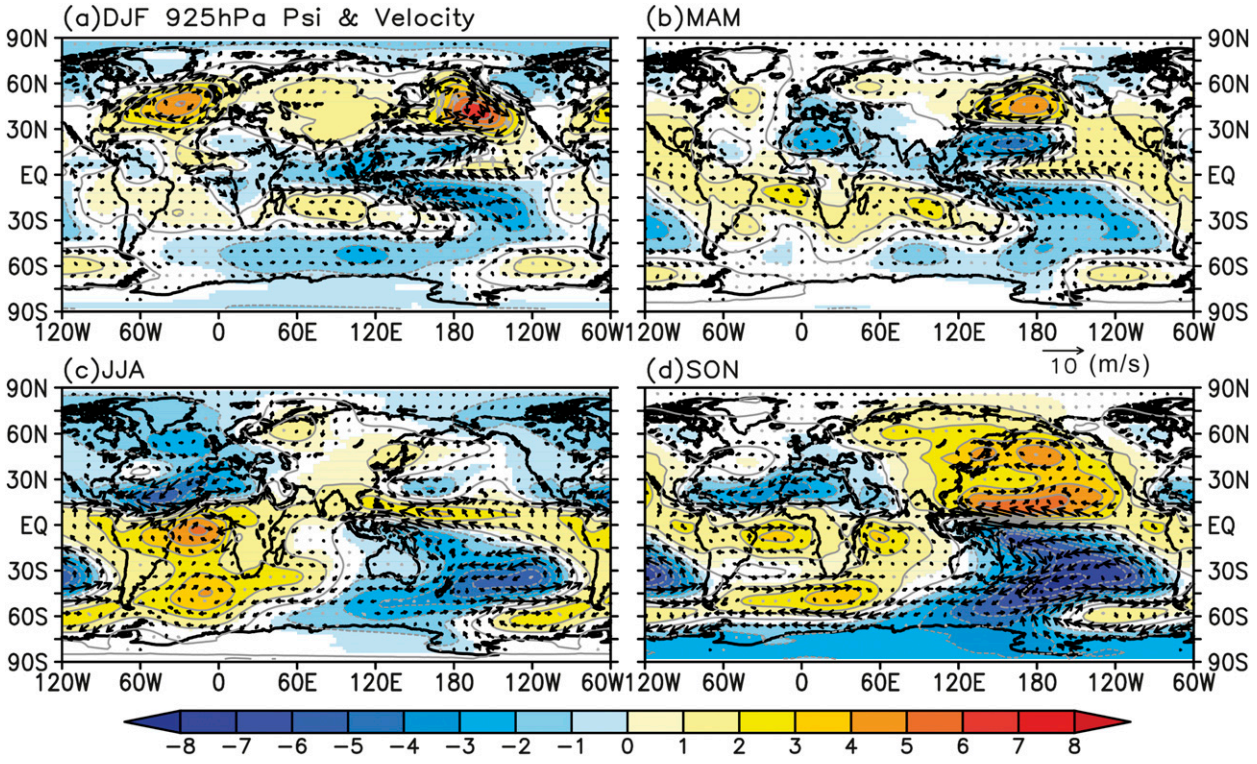

FIG. 11. Differences of seasonal-mean total velocity ($m\,s^{-1}$, arrows) and streamfunction ($m^2\,s^{-1}$, color shading and contours) at 850 hPa between ExpAF and CGCM/SSiB. Regions and vectors where differences are statistically significant at the 95% confidence level are shaded and in dark black, respectively.

dynamics for this model are presented in Lee et al. (2009).

Figures 12a and 12b show the anomalous velocity potential and divergent winds at 250 hPa in the simple model, together with the streamfunction and rotational winds at 750 hPa. With the thermal forcing placed over the African continent, the response of large-scale flows demonstrates the typical equatorial wave solution. The equatorial Kelvin waves extend eastward over the tropical Pacific and modify the intensity of subtropical highs and the equatorial trade winds. Therefore, the equatorial easterlies at low level over the western and central Pacific are enhanced through the anomalous convective heating over Africa. Compared to the differences of large-scale flows between ExpAF and CGCM/SSiB in Figs. 10 and 11, the convection and its associated heating over Africa in ExpAF is enhanced owing to the changes in the LSP. The changes in the large-scale flows at both upper and lower levels are consistent with the responses of this simple model to an anomalous heating source, although the response of Kelvin waves is larger over the Pacific in the CGCM simulations. This feature is likely due to either enhancement by some combination of moist processes within the western Pacific convection zone or by air–sea interaction, as these easterly anomalies produce cold equatorial temperatures. The simple model lacks the convective interactions of moist teleconnections and thus has a simpler response, but it establishes that eastward wave propagation can yield surface easterlies over the equatorial Pacific where they can initiate ocean–atmosphere feedbacks.

We also performed another two simple model tests (Figs. 12d–i) with prescribed heating centers located over South America (~2.5 K day^{-1}, DJF climatological winds) or South and Southeast Asia (~1.25 K day^{-1}, JJA climatological winds). The intensity of heating anomalies approximately corresponds to the heating difference between ExpSA and CGCM/SSiB in DJF or between ExpAA and CGCM/SSiB in JJA, respectively (see Fig. 4). In the South America experiment, the largest impacts of low-level flows are over the equatorial eastern Pacific, Atlantic, and Indian Ocean. The impacts over the western and central Pacific are very small. In the Asia experiment, the impacts of low-level flows are over the equatorial Indian and Pacific Oceans. There are westerly anomalies over the Indian Ocean and easterly anomalies over the Pacific. The easterly anomalies over

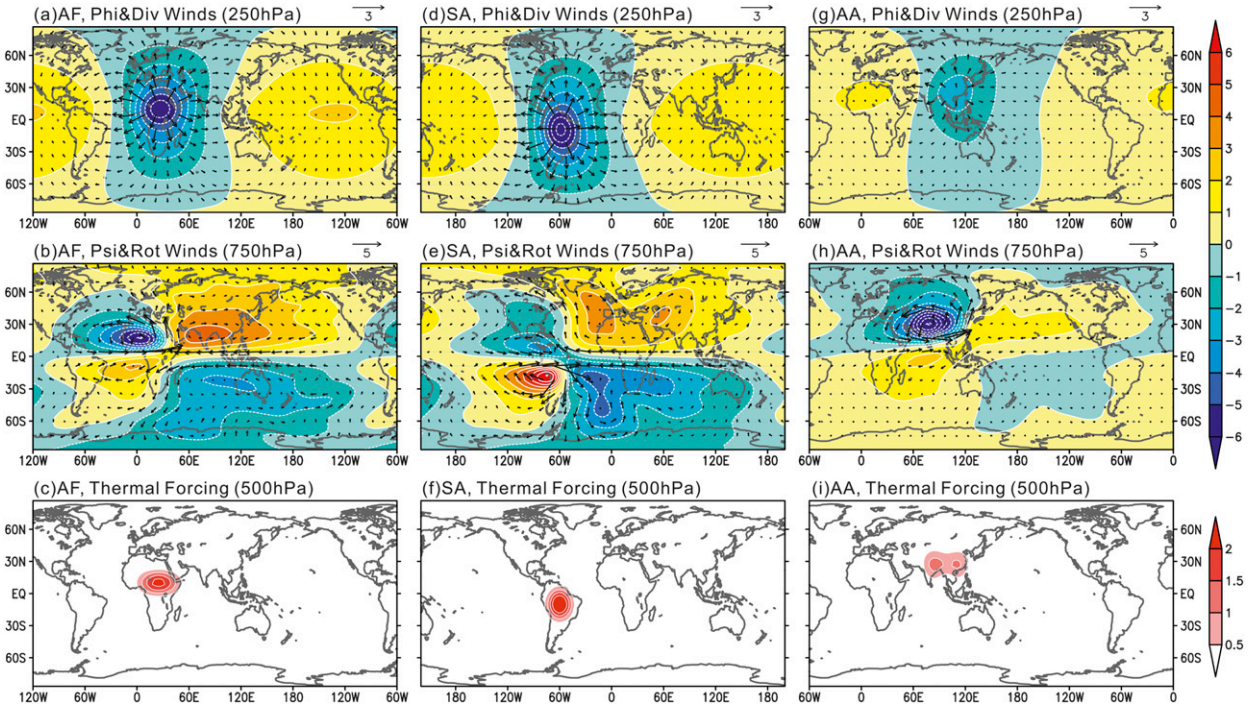

FIG. 12. (a),(d),(g) Anomalous velocity potential ($m^2 s^{-1}$) and divergent winds ($m s^{-1}$) at 250 hPa and (b),(e),(h) streamfunction ($m^2 s^{-1}$) and rotational winds ($m s^{-1}$) at 750 hPa from a two-layer shallow water model with a prescribed thermal forcing (K) at 500 hPa over (c) Africa, (f) South America, and (i) Asia. See text for more details of experimental setup.

the Pacific are consistent with previous modeling studies (Barnett et al. 1989; Meehl 1994; Fu and Wang 2003), but the amplitude is smaller than that in the Africa experiment. This is mostly because the heating is smaller and farther away from the equator.

We further examine the cross section of large-scale flows from the CGCM simulations along the tropics. Figure 13a shows the differences of the JJA zonal component of divergent winds and vertical velocity between ExpAF and CGCM/SSiB averaged over 15°S–15°N. Strong upward motion is present over the tropical African continent and eastern Atlantic sector associated with the anomalous convection. A broad region of sinking motion is present from the western Pacific (120°E) to eastern tropical South America (70°W). At low levels, anomalous easterlies are present over the central and western Pacific Ocean, while anomalous westerlies are present over the tropical Atlantic. The differences in the large-scale flows at upper and lower levels are consistent with those in Figs. 10, 11, and 12. These anomalous low-level flows are consistent with the response of a stronger east–west pressure gradient in the Pacific (120°E–90°W), stronger easterly zonal wind stress in the western to central Pacific (120°E–150°W), and weaker easterly zonal wind stress in the tropical Atlantic (80°–50°W, Fig. 13b). Over the Pacific Ocean, a stronger easterly zonal wind stress resulted in colder SST along the equator.

So far, we have concentrated on JJA. We next examine the seasonal cycles of convective heating over Africa and surface zonal wind stress and SST over the western Pacific. Figure 14 shows the differences of the seasonal cycle (in reference to annual mean) of diabatic heating associated with cumulus convection at 500 hPa over tropical Africa between ExpAF and CGCM/SSiB. The convective heating is strongest north of the equator from July to November. The heating is then weaker in the following seasons, and the maximum is shifting southward following the solar heating with the minimum between November and January. As the convective heating is weaker, the differences in the large-scale circulation in response to the heating are also weaker during the northern winters and springs, as shown in Figs. 10 and 11. The maximum of zonal wind stress is south of the equator between 0° and 10°S and is stronger between July and December and weakest between January and June. The seasonal cycle of the zonal wind stress magnitude over the western Pacific has similar timing to the convective heating magnitude, while the SST is coldest in November and lags behind the wind stress in the Pacific by about one month (Fig. 14b).

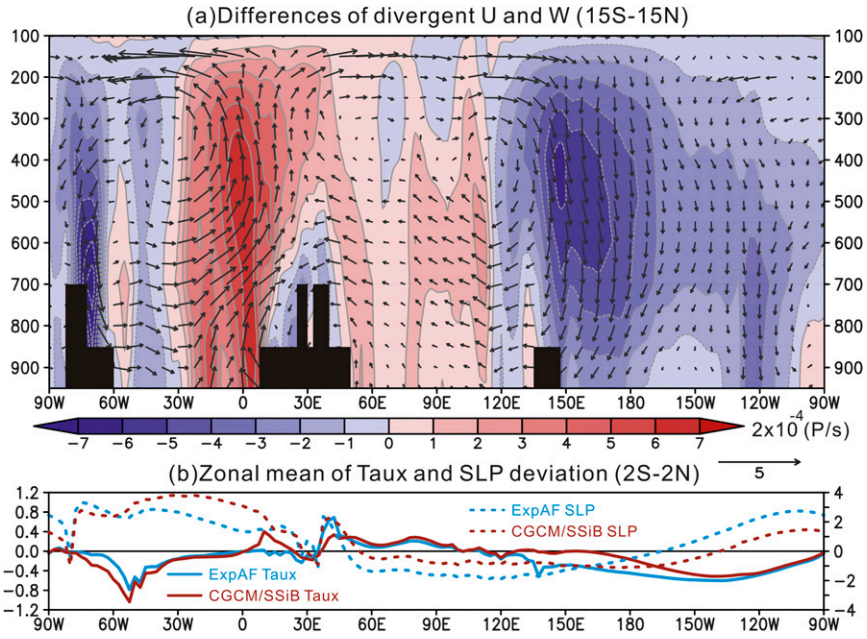

FIG. 13. (a) Differences of June–August divergent zonal winds ($m\,s^{-1}$) and vertical velocity ($Pa\,s^{-1}$) between ExpAF and CGCM/SSiB (ExpAF minus CGCM/SSiB) averaged between 15°S and 15°N. (b) June–August zonal wind stress ($dyn\,cm^{-1}$; $1\,dyn = 10^{-5}\,N$) and deviation sea level pressure from the zonal mean averaged between 2°S and 2°N.

c. *Role of air–sea interactions and ocean memory*

In this subsection, we further discuss the importance of air–sea interactions and ocean memory to the sensitivity revealed by ExpAF. Figure 15 shows the differences of seasonal-mean total velocity and streamfunction at 925 hPa between ExpAFU and AGCM/SSiB (ExpAFU minus AGCM/SSiB). These two experiments are the AGCM-only experiments (Table 1) prescribed with cyclically monthly varying SSTs (Reynolds and Smith 1995) and can be compared with ExpAF and CGCM/SSiB to examine the effects of air–sea interactions. In general, the differences are much smaller compared to those between ExpAF and CGCM/SSiB (Fig. 11). Large differences in the AGCM-only experiments are over the African continent and Atlantic and Indian Ocean basins, while only smaller differences occur over the Pacific. The differences in the easterlies along the equatorial Pacific are only present in JJA and SON. Without air–sea interaction, the response in the subtropical highs in the Pacific is not as significant as those in the CGCM experiments, and the easterlies along the equatorial Pacific in the AGCM experiments are also smaller.

Figure 16 shows the seasonal-mean differences of equatorial upper-ocean temperature (4°S and 4°N) between ExpAF and CGCM/SSiB. In all seasons, subsurface warming occurs in the western Pacific owing to thermocline tilt, and mixed layer cooling occurs associated with increased equatorial upwelling owing to increased easterlies. Interestingly, the differences in the upper-ocean temperature are largest in DJF, while those in surface zonal wind stress and SST are largest in the northern fall. The delay of the response of the upper ocean to surface wind stress anomalies by about one season is as expected from ocean equatorial wave dynamics (e.g., Gill 1982). Furthermore, the colder upper-ocean temperature in ExpAF remains through MAM above 80 m, suggesting that the ocean memory also plays a role in maintaining the colder SST and surface wind stress anomalies when the anomalous convective heating is relatively weaker in the annual cycle in ExpAF.

d. *Discussion*

The mechanisms proposed above involve a series of nonlinear processes taking place in the coupled ocean–atmosphere–land system. As we change the land surface scheme in the CGCM, the land surface fluxes (Bowen ratios or evaporation fraction) also change. The surface fluxes then affect the characteristics of the PBL state. In tropical Africa, the PBL in ExpAF becomes moister and shallower, and deep convection is enhanced. The anomalous heating due to enhanced convection then influences the large-scale circulation over the tropical

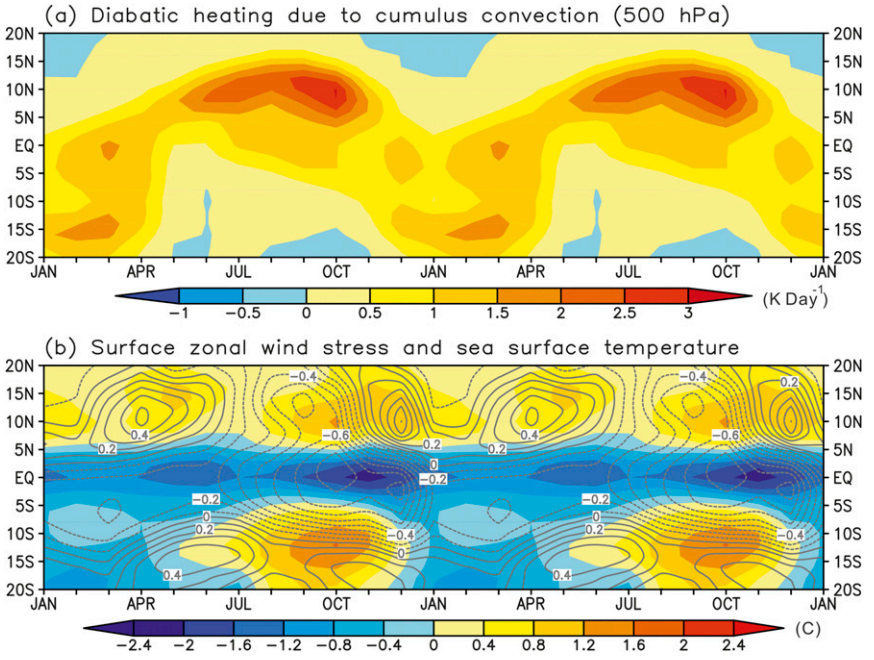

FIG. 14. Differences of annual cycles between ExpAF and CGCM/SSiB (ExpAF minus CGCM/SSiB) for (a) 500-hPa diabatic heating (K day^{-1}) due to cumulus convection averaged over 10°W–50°E and (b) surface zonal wind stress (contours; dyn cm^{-1}) and sea surface temperature (shaded, °C) averaged from 130°E to 150°W.

Pacific including the equatorial easterly trades and surface wind stress through tropical wave dynamics (equatorial Kelvin waves). The strong air–sea coupling in the central Pacific modifies the ocean mean state and the strength of upwelling and thermocline structure along the equator. Ocean memory also plays a role in maintaining the SST anomalies in the following seasons. Based on several previous studies on the tropical Pacific climate (e.g., Dijkstra and Neelin 1995; Neelin et al. 2000; Xiao and Mechoso 2009a,b), the seasonal cycles of SST and interannual variability are sensitive to the climate mean state. In our view, therefore, teleconnections can be amplified by ocean–atmosphere feedbacks within the climatology. As demonstrated in MA13, such indirect effects of land surface processes due to air–sea coupling are significant and have a strong remote impact.

We can also posit that the unique geographic location of the African continent is key to the large impact of perturbations in regional LSP on the tropical Pacific climate. Tropical Africa is characterized by strong land–atmosphere interactions, and therefore convection over that region is sensitive to changes in LSPs. Since the projection of a heating anomaly on equatorial trapped waves is largest for anomalies near the equator, the convection taking place all season long around the equatorial band favors creating equatorial teleconnections. Furthermore, the enhancement of equatorial easterly trades in response to equatorial Kelvin waves has a large impact right along the regions of strong ocean–atmosphere coupling (central equatorial Pacific), which modifies the ocean mean state. The convection over South Asia or northern Australia is farther away from the equator and has stronger seasonality (Fig. 12). Also, the convection over the Amazon in South America is only active during DJF and early March.

Finally, to examine the robustness of our CGCM results, ExpAF was integrated 30 years longer than ExpSA or ExpAA. We compared the results from year 21 to 40 and from year 41 to 70 and found that the mean differences (e.g., precipitation, not shown here) are quite small, and the differences are also smaller than the differences between any LSP experiment and CGCM/SSiB. We also conducted another experiment ExpAFRev in which the model setup in CGCM/SLS is used except that the land surface scheme is replaced by SSiB over the African continent (Table 1), which is designed to further prove that the equatorial tropical climate is sensitive to the LSPs in Africa. Figure 17 presents the differences of annual-mean 500-hPa convective heating, zonal wind stress, SST, and precipitation between ExpAFRev and CGCM/SLS. We can find that, with less convective heating over the tropical African continent, the equatorial easterly trades are weaker and the SST is warmer

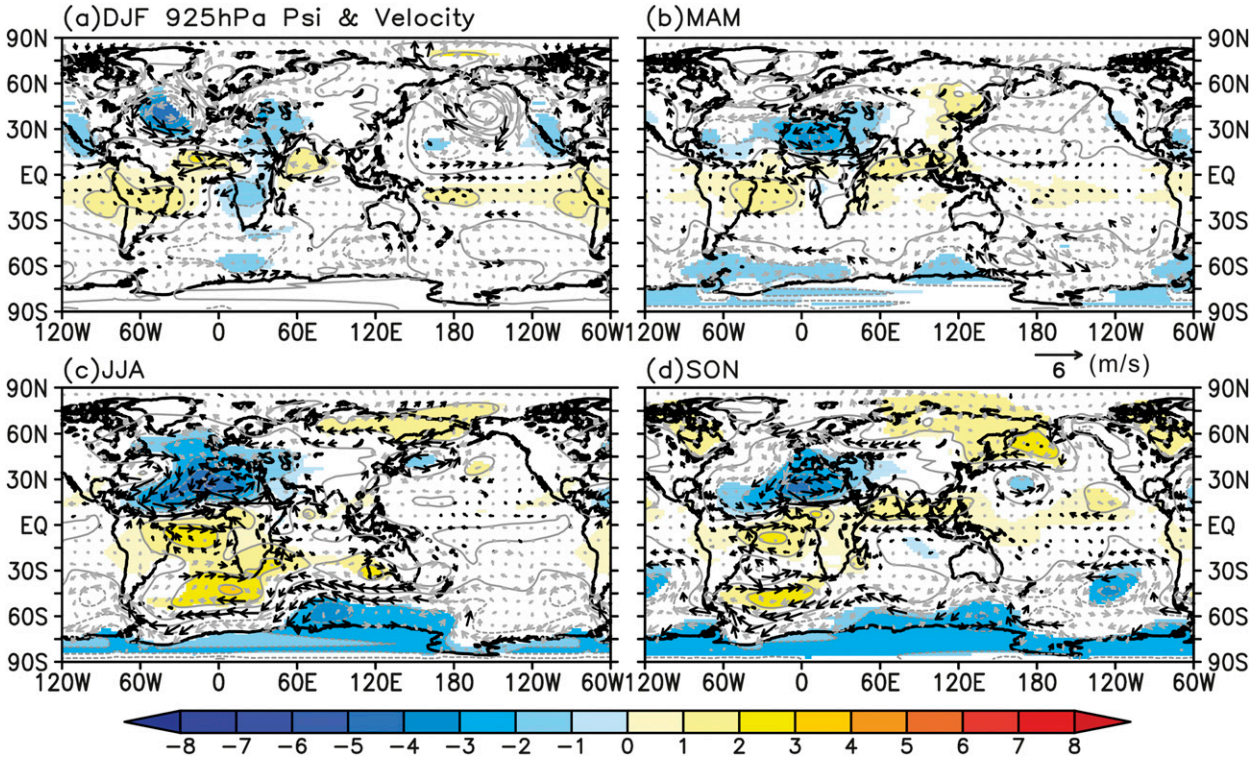

FIG. 15. Differences of seasonal-mean total velocity ($m\,s^{-1}$, arrows) and streamfunction ($m^2\,s^{-1}$, color shading and contours) at 850 hPa between AGCM-only experiments ExpAFU and AGCM/SSiB (ExpAFU minus AGCM/SSiB). Regions and vectors where differences are statistically significant at the 95% confidence level are shaded and in dark black, respectively.

owing to less equatorial upwelling in the ExpAFRev. With warmer SST, more precipitation over the western Pacific warm pool and Maritime Continent are present. In short, the opposite of the response in ExpAF minus CGCM/SSiB is expected. The systematic cold bias of the equatorial cold tongue and too zonally oriented South Pacific convergence zone (SPCZ) are alleviated in the ExpAFRev (Fig. 2) by the retreat of the equatorial cold tongue and strengthening and eastward shift of the heating source associated with warm pool deep convection, explained in works by Kodama (1999) and Rodwell and Hoskins (2001) for subtropical convergence zones.

4. Summary and conclusions

In this study, we examine the effects of continental-scale land surface processes (LSPs) [interactive soil moisture and vegetation biophysical processes (VBP)] on the global tropical climate with an emphasis on the Pacific basin where those effects are found to have larger amplitudes. Our approach is based on simulations from the UCLA AGCM coupled to the MIT OGCM with a simple land scheme (SLS) that specifies surface albedos and soil moisture availability or with the SSiB that allows for interactive soil moisture and VBP. These two processes have a first-order influence on the surface heat and water budgets. Our focus is on the relative impact of the perturbations given by different representation of LSPs in different continental regions. Therefore, we conducted a series of sensitivity experiments in which the land surface scheme was switched from SSiB to SLS (or vice versa) in order to isolate remote impacts from the effects of continental-scale interactive soil moisture and vegetation biophysical processes. The selected continental regions are characterized by strong climate–VBP interactions.

In the global tropics of a coupled ocean–atmosphere–land system, the perturbations associated with different representations of interactive soil moisture and VBP have a strong impact on the seasonal mean state and seasonal cycles of precipitation, clouds, and surface air temperature. According to the results obtained from the series of regional sensitivity experiments, the perturbations over the African continent have the strongest impact. The impacts from the Asian–Australian and South American continents are primarily confined to the local region where the LSP change is prescribed and are

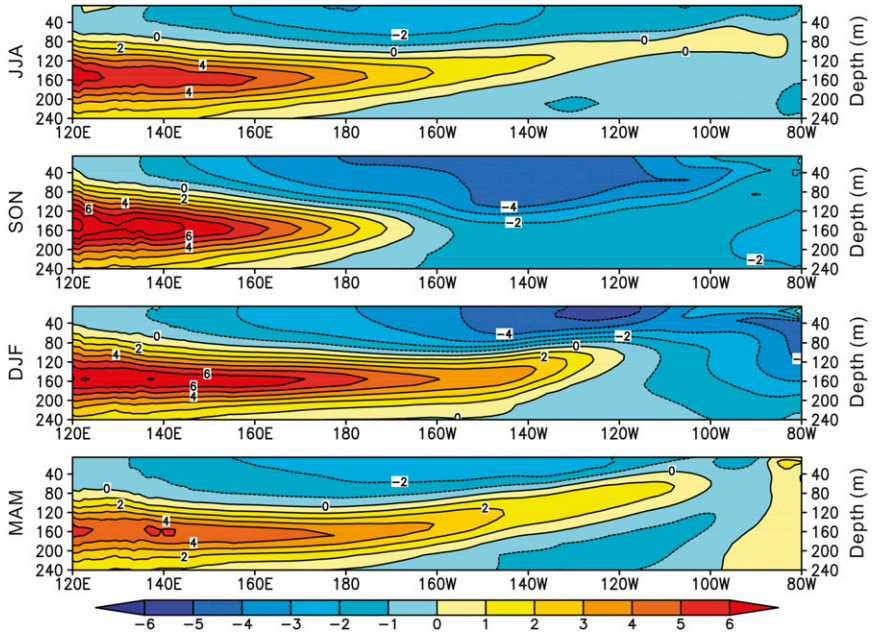

FIG. 16. Differences of the seasonal mean of equatorial upper-ocean temperature (°C, 4°S–4°N) between ExpAF and CGCM/SSiB (ExpAF minus CGCM/SSiB).

secondary or minimal elsewhere. The mechanisms for such impact from LSP perturbations over the African continent are illustrated and summarized in Fig. 18. Convection over tropical Africa is sensitive to the land surface fluxes. In ExpAF, the convection is stronger than that in the CGCM/SSiB owing to increased latent and decreased sensible heat fluxes (lower Bowen ratio and higher evaporation fraction). The enhanced convective heating affects the large-scale circulation through equatorial wave dynamics, as demonstrated by the simple model experiments (Fig. 12). The effects are especially strong in the tropical Pacific where strengthening of the easterly trades and east–west zonal pressure gradient results in enhanced zonal wind stress and equatorial upwelling. Convection differences are stronger during JJA and SON, while the upper-ocean temperature remains colder through DJF and MAM because of the large ocean heat capacity (ocean memory). The colder SST anomalies in the equatorial Pacific can also feed back to the atmosphere and remote regions. The convective heating anomalies associated with LSPs over Asia are smaller and farther from the equator and, hence, do not teleconnect as far. In addition, the heating anomalies over South America only have larger impacts over the eastern Pacific, Atlantic, and Indian Oceans during DJF (Fig. 12).

The differences in convective heating and rainfall over tropical Africa between ExpAF and CGCM/SSiB provided by the different LSP formulations are likely to be on the large side in reference to the observed variability (e.g., Giannini et al. 2008). Nevertheless, we are confident about the usefulness of our results because variability in the observations result from different sources, some of which can act to reduce the total variability. Therefore, the connection between convective heating associated with different LSP representations over the African continent and the tropical Pacific climate discussed here raise several issues. First, such connection suggests that any factors that could cause significant changes in the convective heating over the African continent may also affect the tropical Pacific mean state and variability on a wide range of time scales. Among several possible factors with such a potential impact are land surface flux changes due to land use changes (e.g., deforestation) and the impact from greenhouse gases or aerosols. In addition, the frequency and intensity of El Niño–South Oscillation (ENSO) are sensitive to the tropical Pacific mean state, and the remote impact from ENSO can in turn affect the global climate. If we cannot reasonably represent these effects in climate models, the biases can affect model simulations. Therefore, correctly representing LSPs and land use change and the associated changes in the deep convection over tropical Africa can substantially reduce uncertainty when performing future climate projections under different climate change scenarios.

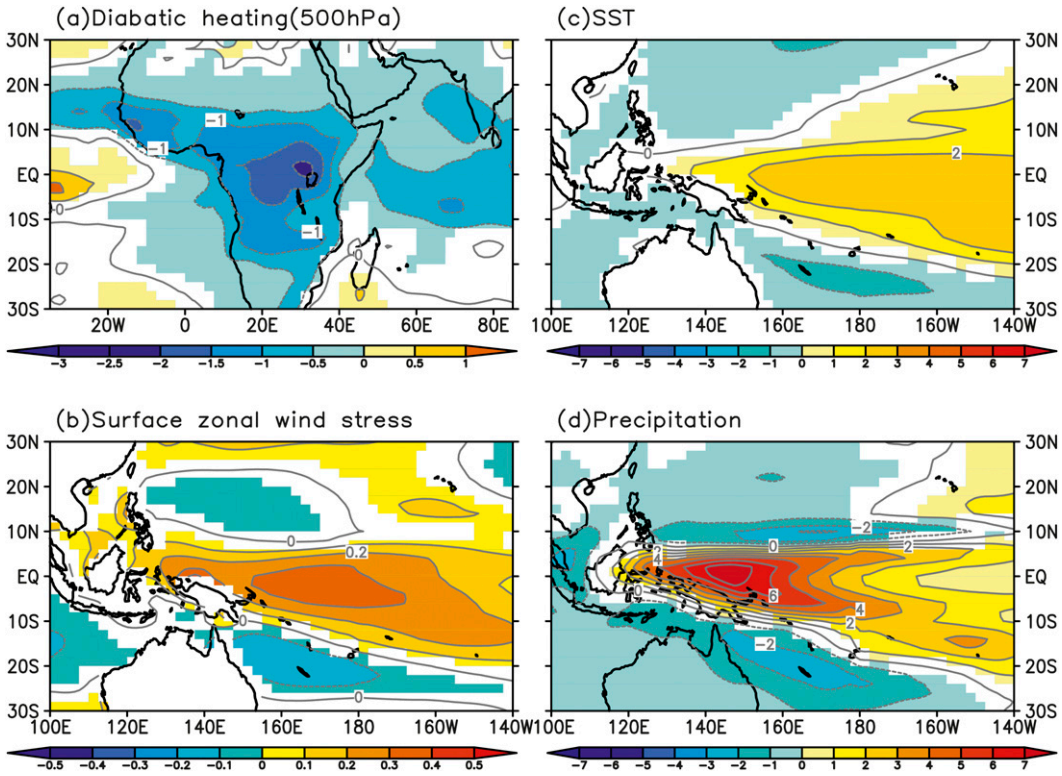

FIG. 17. Differences of annual-mean (a) 500-hPa diabatic heating (K day^{-1}) due to cumulus convection, (b) surface zonal wind stress (contours, dyn cm^{-1}), (c) sea surface temperature (shading, °C), and (d) precipitation (mm day^{-1}) between ExpAFRev and CGCM/SLS (ExpAFRev minus CGCM/SLS). Regions where differences are statistically significant at the 95% confidence level are shaded.

Finally, a better simulation of deep convection in tropical Africa in the CGCM simulations, either through the improvement in the AGCM or land surface model, could also improve overall CGCM performance on the tropical climate, such as the seasonal cycle of SST in the equatorial Pacific, or ENSO, as we demonstrated in ExpAF and ExpAFRev. Furthermore, the cold tongue biases over the western Pacific in almost all contemporary CGCMs could also be improved or alleviated in this regard.

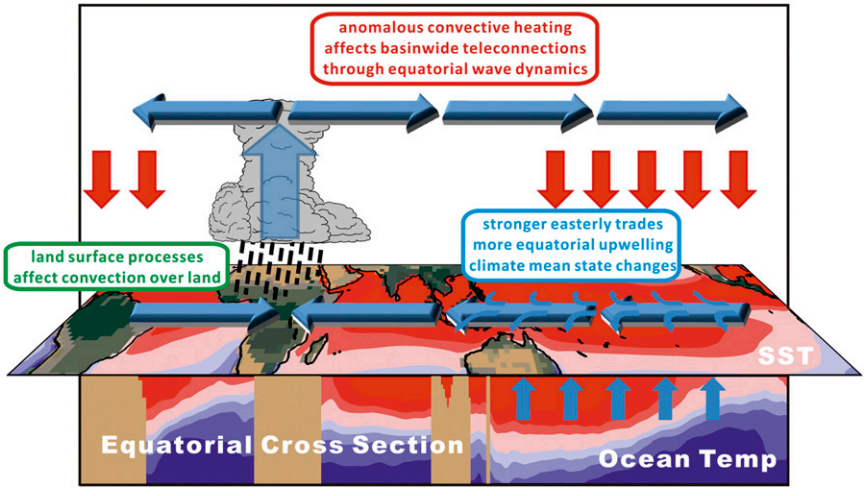

FIG. 18. Schematic diagram for the mechanisms of the connection between the tropical Pacific climate and the LSP over the African continent.

Acknowledgments. We thank three anonymous reviewers for their valuable comments on this paper and Professor Min-Hui Lo for very helpful discussion. Computing resources were provided from the NCAR Computational and Information Systems Laboratory. The contribution of Hsi-Yen Ma to this work was performed under the auspices of the U.S. Department of Energy by Lawrence Livermore National Laboratory under Contract DE-AC52-07NA27344. The Pacific Northwest National Laboratory is operated by the Battelle Memorial Institute for the U.S. Department of Energy under Contract DE-AC05-76RL01830. NOAA's MAPP/CPO program provided support for this work under Grant NA10 0AR4310262. This work was also supported under NSF Grants ATM-0751030, AGS-1041477, AGS-1102838, and AGS-1115506.

APPENDIX

Land Surface Component in the CGCM

The UCLA AGCM currently has two options for a land surface component: one specifies most surface conditions/processes and the other represents interactive land–atmosphere interactions. The key differences between the two schemes representing the land–atmosphere interactions include 1) the representation of surface albedo and 2) the way the surface momentum, heat, and water fluxes are calculated. The first one is a simple land scheme (SLS). In SLS, the surface albedo is cyclically varying monthly climatology obtained from satellite remote sensing. For surface momentum and heat fluxes in SLS, the calculation of bulk aerodynamic formulas of latent and sensible heat fluxes are based on Suarez et al. (1983). The formulations are the same over land and ocean. The efficiency factor β, which represents the ratio of actual and potential evaporation, is prescribed based on observational data, and the spatial adjustments were conducted according to results in long-term integrations (i.e., "tuning," no interactive soil moisture or soil layers). This implies no memory (e.g., deep soil moisture or temperature anomalies) from the land component. Ground temperature (skin temperature) over land is predicted from an energy balance of net surface shortwave radiation, net surface longwave radiation, sensible heat, and latent heat fluxes (no ground heat flux).

As an alternative to the simple land scheme, the AGCM incorporates the first generation of the Simplified Simple Biosphere Model (Xue et al. 1991). This SSiB version has three soil layers and one vegetation layer. Soil moisture of the three soil layers, interception water store for the canopy, deep soil temperature, ground temperature, and canopy temperature are all predicted based on the water and energy balance at canopy and soil. Three aerodynamic resistances control the heat and water fluxes between the canopy layer air space and 1) canopy leaves, 2) soil surface, and 3) the reference PBL height. The resistance values are determined in terms of vegetation properties, ground conditions, and the bulk Richardson number according to the Monin–Obukhov similarity theory (Paulson 1970; Businger et al. 1971; Deardorff 1972; Sellers et al. 1986; Xue et al. 1991, 1996a). The surface albedo is calculated through a two-stream radiative transfer scheme and has diurnal variations representing the change of net solar radiation in the canopy layer due to vegetation properties. Several data sources (Dorman and Sellers 1989; Xue et al. 1996b) have been used to determine the vegetation types that specify monthly climatological land surface properties (e.g., leaf area index, green leaf fraction, and surface roughness length). Over the ocean, calculations of surface momentum, heat, and water fluxes are the same as in the SLS and SSiB. Carbon dioxide and other trace gases remain constant for all of the experiments to simplify the varying processes considered in this study.

REFERENCES

Arakawa, A., 2000: A personal perspective of the early years of general circulation modeling at UCLA. *General Circulation Model Development: Past, Present, and Future,* D. A. Randall, Ed., Academic Press, 1–65.

Barnett, T. P., L. Dumenil, U. Schlese, E. Roeckner, and M. Latif, 1989: The effect of Eurasian snow cover on regional and global climate variations. *J. Atmos. Sci.,* **46,** 661–685.

Boone, A., and Coauthors, 2004: The Rhône-Aggregation Land Surface Scheme intercomparison project: An overview. *J. Climate,* **17,** 187–208.

Businger, J. A., J. C. Wyngaard, Y. Izumi, and E. G. Bradley, 1971: Flux–profile relationships in the atmospheric surface layer. *J. Atmos. Sci.,* **28,** 181–189.

Cazes-Boezio, G., D. Menemenlis, and C. R. Mechoso, 2008: Impact of ECCO ocean-state estimates on the initialization of seasonal climate forecasts. *J. Climate,* **21,** 1929–1947.

Deardorff, J. W., 1972: Parameterization of the planetary boundary layer for use in general circulation models. *Mon. Wea. Rev.,* **100,** 93–106.

Dijkstra, H. A., and J. D. Neelin, 1995: Ocean–atmosphere interaction and the tropical climatology. Part II: Why the Pacific cold tongue is in the east. *J. Climate,* **8,** 1343–1359.

Dorman, J. L., and P. Sellers, 1989: A global climatology of albedo, roughness length and stomatal resistance for atmospheric general circulation models as represented by the Simple Biosphere Model (SiB). *J. Appl. Meteor.,* **28,** 833–855.

Fu, X., and B. Wang, 2003: Influences of continental monsoons and air–sea coupling on the climate of the equatorial Pacific. *J. Climate,* **16,** 3132–3152.

Giannini, A., M. Biasutti, I. M. Held, and A. H. Sobel, 2008: A global perspective on African climate. *Climatic Change,* **90,** 359–383.

Gill, A. E., 1980: Some simple solutions for heat-induced tropical circulation. *Quart. J. Roy. Meteor. Soc.,* **106,** 447–462.

——, 1982: *Atmosphere-Ocean Dynamics.* Academic Press, 662 pp.

Guo, Z.-C., and Coauthors, 2006: GLACE: The Global Land–Atmosphere Coupling Experiment. Part II: Analysis. *J. Hydrometeor.,* **7,** 611–625.

Hales, K., J. D. Neelini, and N. Zeng, 2004: Sensitivity of tropical land climate to leaf area index: Role of surface conductance versus albedo. *J. Climate,* **17,** 1459–1473.

Henderson-Sellers, A., P. Irannejad, K. McGuffie, and A. J. Pitman, 2003: Predicting land-surface climates-better skill or moving targets? *Geophys. Res. Lett.,* **30,** 1777, doi:10.1029/2003GL017387.

Hu, Z.-Z., E. K. Schneider, U. S. Bhatt, and B. P. Kirtman, 2004: Potential mechanism for response of El Niño–Southern Oscillation variability to change in land surface energy budget. *J. Geophys. Res.,* **109,** D21113, doi:10.1029/2004JD004771.

Kalnay, E., and Coauthors, 1996: The NCEP/NCAR 40-Year Reanalysis Project. *Bull. Amer. Meteor. Soc.,* **77,** 437–471.

Kodama, Y. M., 1999: Roles of the atmospheric heat sources in maintaining the subtropical convergence zones: An aquaplanet GCM study. *J. Atmos. Sci.,* **56,** 4032–4049.

Koster, R. D., and Coauthors, 2004: Regions of strong coupling between soil moisture and precipitation. *Science,* **305,** 1138–1140, doi:10.1126/science.1100217.

——, and Coauthors, 2006: GLACE: The global land–atmosphere coupling experiment. Part I: Overview. *J. Hydrometeor.,* **7,** 590–610.

Lee, S.-K., C. Wang, and B. Mapes, 2009: A simple atmospheric model of the local and teleconnection responses to heating anomalies. *J. Climate,* **22,** 272–284.

Ma, H.-Y., C. R. Mechoso, Y. Xue, H. Xiao, C.-M. Wu, J.-L. Li, and F. De Sales, 2010: Impact of land surface processes on the South American warm season climate. *Climate Dyn.,* **37,** 187–203, doi:10.1007/s00382-010-0813-3.

——, H. Xiao, C. R. Mechoso, and Y. Xue, 2013: Sensitivity of global tropical climate to land surface processes: Mean state and interannual variability. *J. Climate,* **26,** 1818–1837.

Marshall, J., A. Adcroft, C. Hill, L. Perelman, and C. Heisey, 1997: A finite-volume, incompressible Navier Stokes model for studies of the ocean on parallel computers. *J. Geophys. Res.,* **102** (C3), 5753–5766.

Martin, G. M., and R. C. Levine, 2012: The influence of dynamic vegetation on the present-day simulation and future projections of the South Asian summer monsoon in the HadGEM2 family. *Earth Syst. Dyn.,* **3,** 245–261.

Mechoso, C. R., J.-Y. Yu, and A. Arakawa, 2000: A coupled GCM pilgrimage: From climate catastrophe to ENSO simulations. *General Circulation Model Development: Past, Present and Future,* D. A. Randall, Ed., Academic Press, 539–575.

Meehl, G. A., 1994: Influence of the land surface in the Asian summer monsoon: External conditions versus internal feedbacks. *J. Climate,* **7,** 1033–1049.

Neelin, J. D., F.-F. Jin, and H.-H. Syu, 2000: Variations in ENSO phase locking. *J. Climate,* **13,** 2570–2590.

Notaro, M., S. Vavrus, and Z. Liu, 2007: Global vegetation and climate change due to future increases in CO_2 as projected by a fully coupled model with dynamic vegetation. *J. Climate,* **20,** 70–90.

Paulson, C. A., 1970: Mathematical representation of wind speed and temperature profiles in the unstable atmospheric surface layer. *J. Appl. Meteor.,* **9,** 857–861.

Reynolds, R. W., and T. M. Smith, 1995: A high-resolution global sea surface temperature climatology. *J. Climate,* **8,** 1571–1583.

Richter, I., S.-P. Xie, A.T. Wittenberg, and Y. Masumoto, 2012: Tropical Atlantic biases and their relation to surface wind stress and terrestrial precipitation. *Climate Dyn.,* **38,** 985–1001, doi:10.1007/s00382-011-1038-9.

Rodwell, M. J., and B. J. Hoskins, 2001: Subtropical anticyclones and summer monsoons. *J. Climate,* **14,** 3192–3211.

Sellers, P. J., Y. Mintz, Y. C. Sud, and A. Dalcher, 1986: A Simple Biosphere Model (SiB) for use within general circulation models. *J. Atmos. Sci.,* **43,** 505–531.

Seneviratne, S. I., D. Lüthi, M. Litschi, and C. Schär, 2006: Land-atmosphere coupling and climate change in Europe. *Nature,* **443,** 205–209.

Smith, T. M., R. W. Reynolds, T. C. Peterson, and J. Lawrimore, 2008: Improvements to NOAA's historical merged land–ocean surface temperature analysis (1880–2006). *J. Climate,* **21,** 2283–2296.

Suarez, M. J., A. Arakawa, and D. A. Randall, 1983: The parameterization of the planetary boundary layer in the UCLA general circulation model: Formulation and results. *Mon. Wea. Rev.,* **111,** 2224–2243.

Swann, A. L. S., I. Y. Fung, and J. C. H. Chiang, 2011: Mid-latitude afforestation shifts general circulation and tropical precipitation. *Proc. Natl. Acad. Sci. USA,* **109,** 712–716.

Wang, C., S.-K. Lee, and C. R. Mechoso, 2010: Interhemispheric influence of the Atlantic warm pool on the southeastern Pacific. *J. Climate,* **23,** 404–418.

Wei, J., and P. A. Dirmeyer, 2010: Toward understanding the large-scale land-atmosphere coupling in the models: Roles of different processes. *Geophys. Res. Lett.,* **37,** L19707, doi:10.1029/2010GL044769.

——, ——, and J. Zhang, 2010: Land-caused uncertainties in climate change simulations: A study with the COLA AGCM. *Quart. J. Roy. Meteor. Soc.,* **136,** 819–824.

Xiao, H., and C. R. Mechoso, 2009a: Correlative evolutions of ENSO and the seasonal cycle. *J. Atmos. Sci.,* **66,** 1041–1049.

——, and ——, 2009b: Seasonal cycle–El Niño relationship: Validation of hypotheses. *J. Atmos. Sci.,* **66,** 1633–1653.

Xie, P., and P. A. Arkin, 1997: Global precipitation: A 17-year monthly analysis based on gauge observations, satellite estimates, and numerical model outputs. *Bull. Amer. Meteor. Soc.,* **78,** 2539–2558.

Xue, Y., P. J. Sellers, J. L. Kinter III, and J. Shukla, 1991: A simplified biosphere model for global climate studies. *J. Climate,* **4,** 345–364.

——, H. G. Bastable, P. A. Dirmeyer, and P. J. Sellers, 1996a: Sensitivity of simulated surface fluxes to changes in land surface parameterization—A study using ABRACOS data. *J. Appl. Meteor.,* **35,** 386–400.

——, M. J. Fennessy, and P. J. Sellers, 1996b: Impact of vegetation properties on U.S. summer weather prediction. *J. Geophys. Res.,* **101** (D3), 7419–7430.

——, H.-M. H. Juang, W. Li, S. Prince, R. DeFries, Y. Jiao, and R. Vasic, 2004: Role of land surface processes in monsoon development: East Asia and West Africa. *J. Geophys. Res.,* **109,** D03105, doi:10.1029/2003JD003556.

——, F. De Sales, W. Li, C. R. Mechoso, C. Nobre, and H.-M. H. Juang, 2006: Role of land surface processes in South American monsoon development. *J. Climate,* **19,** 741–762.

——, ——, R. Vasic, C. R. Mechoso, S. D. Prince, and A. Arakawa, 2010: Global and temporal characteristics of seasonal climate/vegetation biophysical process (VBP) interactions. *J. Climate,* **23,** 1411–1433.

Zeng, N., and J. D. Neelin, 1999: A land–atmosphere interaction theory for the tropical deforestation problem. *J. Climate,* **12,** 857–872.

——, R. E. Dickinson, and X. Zeng, 1996: Climatic impact of Amazon deforestation—A mechanistic model study. *J. Climate,* **9,** 859–883.